



Optical and Electrochemical Properties of Self-Organized TiO₂ Nanotube Arrays From Anodized Ti–6Al–4V Alloy

Henia Fraoucene¹, Vinsensia Ade Sugjawati², Djedjiga Hatem¹, Mohammed Said Belkaid¹, Florence Vacandio^{2*}, Marielle Eyraud², Marcel Pasquinelli³ and Thierry Djenizian⁴

¹ Laboratory of Advanced Technologies of Genie Electrics, Faculty of Electrical and Computer Engineering Mouloud Mammeri University, Tizi-Ouzou, Algeria, ² Electrochemistry of Materials Research Group, Aix-Marseille Université, CNRS, MADIREL, UMR 7246, Marseille, France, ³ Optoelectronics and Photovoltaics (OPTO-PV) Team, Institute of Microelectronic Materials Nanosciences of Provence (IM2NP), St Jérôme Center, University of Provence, Marseille, France, ⁴ Mines Saint-Etienne, Department of Flexible Electronics, Center of Microelectronics in Provence, Gardanne, France

OPEN ACCESS

Edited by:

Jean-Michel Lavoie,
Université de Sherbrooke, Canada

Reviewed by:

Xiao-Yu Wu,
Massachusetts Institute of
Technology, United States
Zhibao Huo,
Shanghai Jiao Tong University, China

*Correspondence:

Florence Vacandio
florence.vacandio@univ-amu.fr

Specialty section:

This article was submitted to
Chemical Engineering,
a section of the journal
Frontiers in Chemistry

Received: 25 October 2018

Accepted: 23 January 2019

Published: 08 February 2019

Citation:

Fraoucene H, Sugjawati VA, Hatem D, Belkaid MS, Vacandio F, Eyraud M, Pasquinelli M and Djenizian T (2019) Optical and Electrochemical Properties of Self-Organized TiO₂ Nanotube Arrays From Anodized Ti–6Al–4V Alloy. *Front. Chem.* 7:66. doi: 10.3389/fchem.2019.00066

Due to their high specific surface area and advanced properties, TiO₂ nanotubes (TiO₂ NTs) have a great significance for production and storage of energy. In this paper, TiO₂ NTs were synthesized from anodization of Ti-6Al-4V alloy at 60 V for 3 h in fluoride ethylene glycol electrolyte by varying the water content and further annealing treatment. The morphological, structural, optical and electrochemical performances of TiO₂ NTs were investigated by scanning electron microscope (SEM), energy dispersive X-ray spectroscopy (EDS), X-ray diffraction (XRD), UV-Visible spectroscopy and electrochemical characterization techniques. By varying the water content in the solution, a honeycomb and porous structure was obtained at low water content and the presence of ($\alpha + \beta$) phase in Ti-6Al-4V alloy caused not uniform etching. With an additional increase in water content, a nanotubular structure is formed in the ($\alpha + \beta$) phases with different morphological parameters. The anatase TiO₂ NTs synthesized with 20 wt% H₂O shows an improvement in absorption band that extends into the visible region due the presence of vanadium oxide in the structure and the effective band gap energy (E_g) value of 2.25 eV. The TiO₂ NTs electrode also shows a good cycling performance, delivering a reversible capacity of 82 mAh.g⁻¹ (34 μ Ah.cm⁻². μ m⁻¹) at 1C rate over 50 cycles.

Keywords: TiO₂ nanotubes, Ti-6Al-4V alloy, anodization, Li-ion microbatteries, negative electrode

INTRODUCTION

Rechargeable batteries play an important role in powering the electronic devices and in storing energy due to their high energy and power density which are expected to be a solution for the future energy storage requirements (Li et al., 2017). Due to the lack of suitable on-board power sources, the advances in the miniaturization of microelectronics is growing, opening opportunities to explore the both cathode and anode materials as thin-films (Sugjawati et al., 2016) and nanostructured electrodes by utilizing various synthesis and deposition techniques (Djenizian et al., 2011; Pikul et al., 2013; Ellis et al., 2014; Xiong et al., 2014; Sugjawati et al., 2018).

Titanium dioxide (TiO₂) is a semiconductor material that has been studied extensively in the last few decades due to its chemical stability, non-toxicity and biocompatibility (Morozová et al., 2012; Pansila et al., 2012; Reszczynska et al., 2014). In Li-ion microbatteries, the electrochemical performances of anode materials are highly dependent on their morphologies, surface characteristics, and particle sizes. Many researchers proposed to reduce the size of TiO₂ anode material to the nanometer scale in order to increase not only the number of reaction sites, but also gives new properties to the materials (Armstrong et al., 2005). Among these nanostructured materials, self-organized TiO₂ nanotubes (TiO₂ NTs) obtained by anodization of Ti foil can give a high porosity and larger specific area offering an enhancement in the cell capacity and cycle life (Ortiz et al., 2008, 2009; Fang et al., 2009; Panda et al., 2012; Kyeremateng et al., 2013b; Plylahan et al., 2014; Chang et al., 2015; Salian et al., 2017).

In addition, physical and electrochemical performance of TiO₂ NTs can be enhanced by chemical modification of the surface (Plylahan et al., 2012; Kyeremateng et al., 2013a; Sopha et al., 2017) and by incorporation of foreign ions into TiO₂ lattice such as Sn⁴⁺ (Kyeremateng et al., 2013b), Fe³⁺ (Das et al., 2011), Ni²⁺ (Choi et al., 2009), Nb⁵⁺ (Salian et al., 2018), and V³⁺ (Lin et al., 2013). The electrical conductivity and electrochemical kinetics of TiO₂ NTs electrodes can be improved by doping with Ti³⁺ ions due to a Li⁺ diffusion coefficient of $1.09 \times 10^{-12} \text{ cm}^2 \text{ s}^{-1}$ which is almost one order of magnitude higher than that of TiO₂ NTs ($1.39 \times 10^{-13} \text{ cm}^2 \text{ s}^{-1}$) (Duan et al., 2016). Yu et al. also demonstrated that 5 at.% Sn doped TiO₂ NTs exhibits the best cycling stability with specific capacity of 386 mAh.g⁻¹ and coulombic efficiency of 99.2% after 50 cycles at 0.1C (Yu et al., 2014).

Ternary titanium alloy (Ti-6Al-4V, with 6 wt% Aluminum and 4 wt% Vanadium) have also been utilized to synthesize the self-organized TiO₂ NTs, notably for their use in a wide range of applications such as bone substitute applications, including orthopedic and dental implants due to their superior compatibility, mechanical resistance, excellent corrosion resistance, and good thermal stability (Long and Rack, 1998; Black and Hastings, 2013). Furthermore, research works focused to improve the osseointegration and stability of the TA6V implant in the human body (Jo et al., 2013). However, to the best of our knowledge, there have been no reports to date on the use of the anodized TA6V alloy as electrode for Li-ion microbatteries. The basic objective of this work is therefore to study the electrochemical performance and optical properties of the anodized TA6V alloy produced through electrochemical anodization in fluoride-containing ethylene glycol electrolyte.

EXPERIMENTAL

Synthesis of TiO₂ Nanotubes

The Ti–6Al–4V (TA6V) alloy (0.1 mm thickness, 25% tolerance, Goodfellow) were cut into square shape ($1.2 \times 1.2 \text{ cm}$) with a selected work area of 0.6 cm^2 . Before anodization, the Ti–6Al–4V foils were degreased by sonication in acetone, 2-propanol and methanol for 10 min each, rinsed with ultrapure water and dried in a stream of compressed air. The anodization

was performed in a two-electrode electrochemical cell with Ti–6Al–4V foil as the anode and platinum foil as the cathode. At room temperature, all anodization experiments were carried out under a constant voltage of 60 V using a generator (ISO-TECH IPS-603) for 3 h. Ethylene glycol (EG) solution containing 0.3 wt% ammonium fluoride (NH₄F) was used as electrolyte, and the water content was varied at 2, 5, 10, 15, and 20 wt%. After anodization, the samples were soaked in ultrapure water for 10 min and then dried in an oven at 50°C for 10 min. In order to transform the amorphous crystallographic structure obtained just after electrochemical anodization into crystalline structure, the samples were annealed at 500°C for 3 h with a heating and cooling rate of 5°C/min.

Characterization of the Samples

Morphological characterization of the TiO₂ NTs was investigated by scanning electron microscopy (SEM) using a PHILIPS XL30. The chemical composition was analyzed by energy dispersive X-ray spectroscopy (EDS). The crystalline phases were characterized by X-ray diffraction (XRD) analysis. The diffraction patterns were obtained by a X'Pert Philips MPD with a Panalytical X'Celerator detector using a graphite monochromized CuK α radiation ($\lambda = 1.5418 \text{ \AA}$). The measurements were performed within the range of 2θ from 20° to 70°. The optical properties were investigated using a UV-Visible spectroscopy from 250 to 800 nm.

The electrochemical performance tests were performed using two-electrode Swagelok cells assembled in an argon-filled glove box in which the oxygen and moisture contents were <2 ppm. A 9 mm diameter Li foil was used as the counter electrode and two sheets of Whatman glass microfiber separator were soaked in the electrolyte of lithium hexafluorophosphate in ethylene carbonate and diethylene carbonate electrolyte (1M LiPF₆ in EC/DEC of 1:1 w/w) purchased from Sigma-Aldrich prior to assembling the cell. The cycling experiments were performed using a VMP3 potentiostat-galvanostat (Biologic, France). For all experiments, no additives such as poly (vinyl difluoride) as binder and carbon black as conductive agent were utilized. Cyclic voltammetry (CV) measurements were performed in the range voltage of 1–3 V vs. Li/Li⁺ at a scan rate of 0.05, 0.1 and 0.5 mV.s⁻¹, respectively. For galvanostatic discharge-charge tests, a constant current density of 3.23 $\mu\text{A.cm}^{-2}$ (C/10), 6.47 $\mu\text{A.cm}^{-2}$ (C/5), 16.18 $\mu\text{A.cm}^{-2}$ (C/2), and 32.35 $\mu\text{A.cm}^{-2}$ (1C), respectively, was applied to the assembled cells with a cut-off potential of 1–3 V vs. Li/Li⁺.

EXPERIMENTAL RESULTS

Morphological and Chemical

Characterization

Surface Morphology

Figure 1 shows the SEM images of the different morphologies of TA6V alloy anodized at 60 V for 3 h in Ethylene Glycol (EG) solution containing 0.3 wt% NH₄F with different water contents. It should be noticed that the ternary titanium alloy studied in the present work consist of two metallurgical phases, the α phase being enriched in Al and the β phase in V (Macak et al., 2005). We noted a great influence of the water content on

the formation of the self-organized TiO₂ NTs, both randomly arranged porous structure and uniformly arranged nanotubes. The formation of the porous structure depends on the underlying

phase (α or β) and the anodization parameters. As seen in **Figure 1A**, a honeycomb is obviously formed on the surface at water content of 2 wt%, however not on the entire surface.

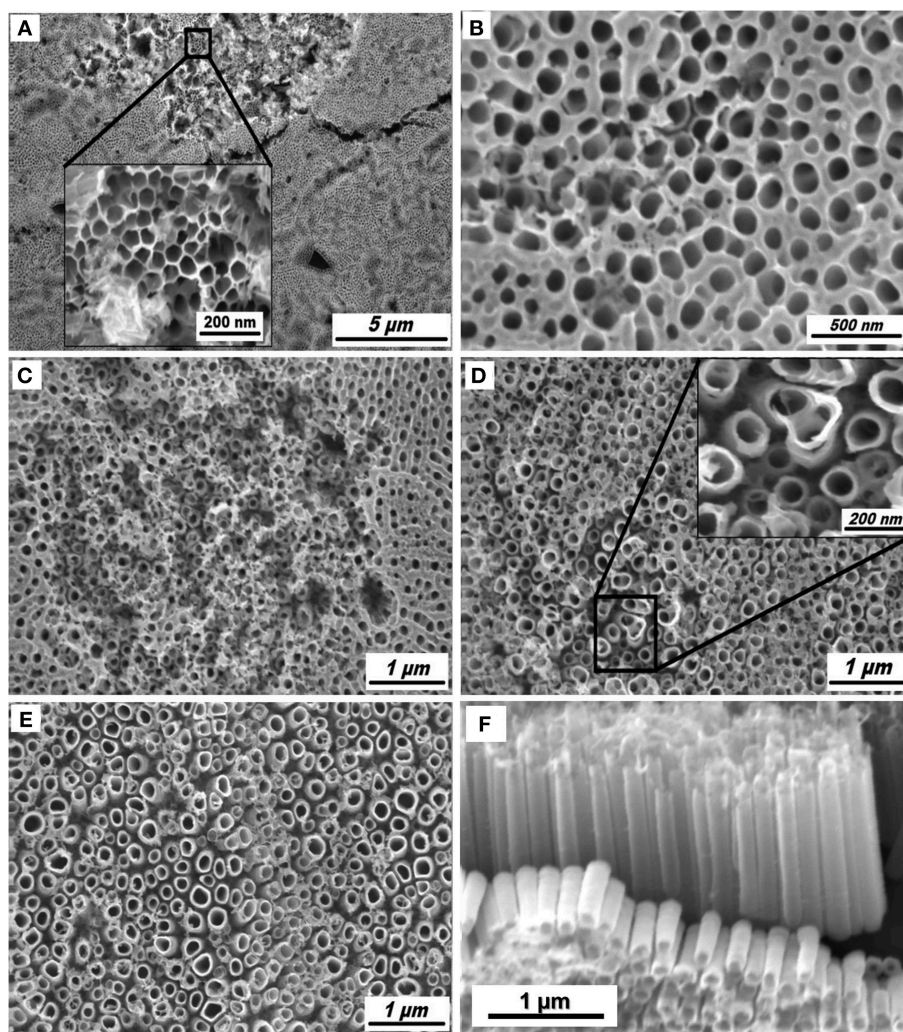


FIGURE 1 | SEM images of TiO₂ NTs obtained from anodization of TA6V alloy in fluoride ethylene glycol electrolyte with different water contents: 2 wt% **(A)**, 5 wt% **(B)**, 10 wt% **(C)**, 15 wt% **(D)**, and 20 wt% **(E)**. Tilted view of TiO₂ NTs synthesized in 20 wt% H₂O **(F)**.

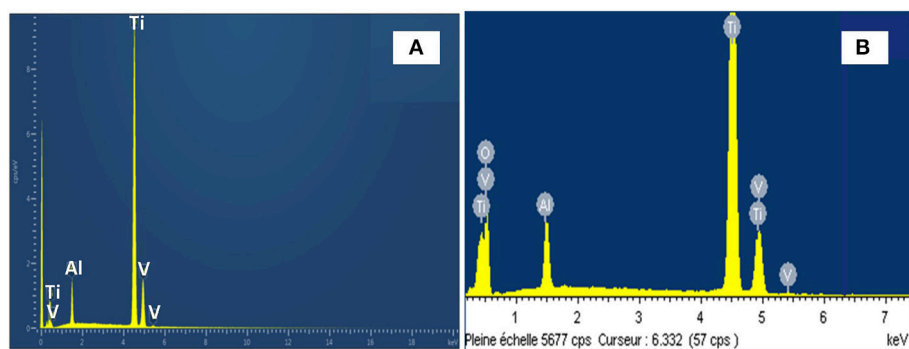


FIGURE 2 | EDS spectra of: pristine TA6V alloy **(A)** and anodized TA6V alloy in fluoride ethylene glycol electrolyte with 20 wt% H₂O content **(B)**.

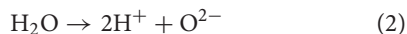
TABLE 1 | Elemental composition of the pristine TA6V alloy and the anodized TA6V alloy obtained in fluoride ethylene glycol electrolyte carrying 20 wt% H₂O content.

| Element | % Weight | | % Atomic | |
|---------|---------------------|---------------------|---------------------|---------------------|
| | Pristine TA6V alloy | Anodized TA6V alloy | Pristine TA6V alloy | Anodized TA6V alloy |
| Al | 6.41 | 3.61 | 10.87 | 3.95 |
| V | 3.21 | 2.68 | 2.88 | 1.55 |
| O | – | 29.93 | – | 55.21 |
| Ti | 90.37 | 63.78 | 86.25 | 39.29 |

Figures 1B–D exhibits the positive influence of the improved water content, from 5 to 15 wt%. The β phase is preferentially etched as the amount of water in the solution increases, indicating the enhanced solubility of the vanadium oxides. A similar phenomenon has been previously reported for the TiO₂ NTs grown from anodization of TA6V alloy in different electrolytes (sulphuric/hydrofluoric acid and ammonium sulfate with 0.2 wt% NH₄F, respectively) at controlled voltage and anodization time (Matykina et al., 2011; Moravec et al., 2016). According to **Figures 1E,F**, a well-separated TiO₂ NTs with an inner diameter varying between 97 and to 206 nm and a length of 1.25 μ m can be formed in the fluoride-containing EG electrolyte carrying 20 wt% H₂O. At this percentage, the nanotubular structure is formed in the two phases ($\alpha + \beta$) via the formation of an oxide layer (TiO₂) and the chemical dissolution of this layer assisted by an electric field. The formation mechanism of TiO₂ NTs from alloys is similar to that of the pristine TiO₂ NTs obtained from anodization of pure Ti.

Composition Analysis

Figure 2 shows the EDS spectra of TiO₂ NTs grown from anodization of TA6V alloy with 20 wt% H₂O content in the fluoride EG. The energy dispersive X-ray characterization values are summarized in **Table 1**. After anodization, there is a slight difference of wt% for each element and the strong presence of oxygen confirming the formation of oxides. In fact, the wt% of Ti in the anodized TA6V alloy is lower compared to that of the pristine TA6V alloy. This result suggests that Ti anode is oxidized into TiO₂ through the oxidation of Ti to form Ti⁴⁺ according to Equation (1).



The dissociation of H₂O takes place at the cathode (Equation 2) and the overall reaction leads to the formation of the titanium dioxide (Equations 3 and 4) (Ortiz et al., 2009). TiO₂ NTs formed in the fluoride electrolyte are characterized by different morphological parameters (diameter, thickness, length,...) that can be confirmed from **Figures 1E,F**.

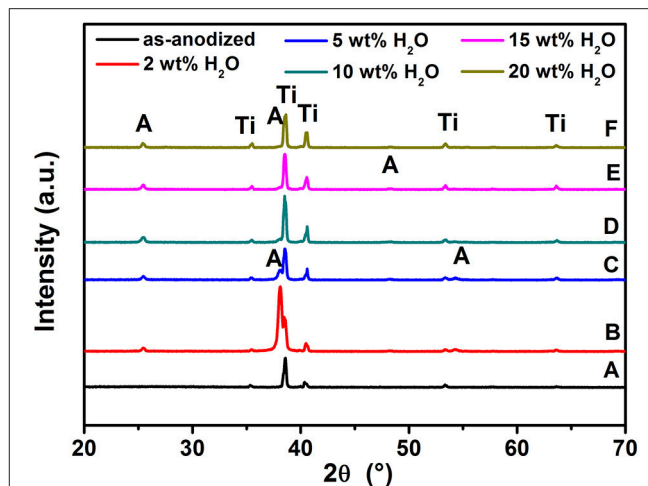


FIGURE 3 | XRD patterns of TiO₂ NTs grown on TA6V alloy: as-anodized (A), films annealed at 500°C for 3 h with the water content in the electrolyte is: 2 wt% H₂O (B), 10 wt% H₂O (C), 5 wt% H₂O (D), 15 wt% H₂O (E), and 20 wt% H₂O (F). "A" is Anatase, "Ti" is substrate of film.

The EDS analysis also shows that Al and V values are lower compared to the TA6V alloy, which can be explained by the oxidation of these elements to form the thin oxide layers of Al₂O₃ and V₂O₅ (or VO₂), respectively (Gibran et al., 2018). Note that Al and V signals may come also from the bulk alloy, not only from the surface oxide layer (Benea et al., 2014). The presence of these layers improves the osseointegration and enhances the biocompatibility of the implant material (Jo et al., 2013). It can be noted that no trace of F can be detected suggesting that this element is not incorporated into the oxides during the anodization process.

Structural Properties

After anodization, the as-formed TiO₂ NTs at various water contents were annealed at 500°C for 3 h to convert the amorphous compound into a crystalline structure. **Figure 3** shows the XRD patterns of these films. Compared to the as-anodized TiO₂ NTs using 20 wt% H₂O, the crystallizations of the TiO₂ NTs films are mainly composed of anatase phase, as evidenced by the diffraction peaks at $2\theta = 25.50, 37.80, 48.30,$ and 55.10° . The diffraction peaks can be indexed to the (101), (004), (200), and (211) planes, respectively (JCPDS Pattern no 00-021-1272). Furthermore, the XRD patterns give no indication of the presence of the Al₂O₃ and V₂O₅ (or VO₂) peaks due to their low percentage in the samples and the high dispersion of metal ions in the nanotubular lattice (Li et al., 2009; Tang et al., 2014).

Optical Properties

Figures 4A–E shows the optical absorption spectra of the annealed TiO₂ NTs at 500°C for 3 h obtained from anodization of TA6V alloy in fluoride EG electrolyte at different water contents. The strong absorptions of these films in the range of 250–336 nm correspond to the electron-transition from the valence band (VB) to the conduction band (CB) with creation of two very

reactive species, an electron in the CB and a hole in the VB (Hoffmann et al., 1995). The UV absorption edge of samples prepared using 2, 5, 10, 15, and 20 wt% H₂O that are around 332, 335, 340, 380, and 410 nm, respectively, correspond to the maximum absorption edge for each curves that are projected on the wavelength axis (nm). By increasing the water content in the solution, the absorption band extends into the visible region. This behavior explained by the increase of the active surface (number of reaction sites) with the formation of TiO₂ NTs characterized by an improvement of their morphological parameters (diameter, thickness, length...) confirmed by the SEM images given in **Figures 1E,F**. In addition, the presence of vanadium oxide in the structure is responsible for additional impurity states in the band gap near the CB or the VB altering the optical properties of the material (Li et al., 2009; Nešić et al., 2013; Chen et al., 2015). The same behavior was obtained by the study of Luo et al. suggesting that the extends of absorption edge into the visible region is attributed to the quantum size effects (Luo et al., 2008).

Evaluation of the TiO₂ NTs band gap (E_g) grown from anodization of Ti–6Al–4V alloy can be obtained from the absorption coefficient α given in Equation (5) (Mane et al., 2005)

$$\alpha = (h\nu - E_g)^{0.5}/h\nu \quad (5)$$

$\alpha = A / l$, where A is the absorption film, l is the tubes length ($l = 1.25 \mu\text{m}$) and $h\nu$ is the photon energy. **Figure 4F** shows the variations of $(\alpha h\nu)^2$ vs. photon energy ($h\nu$) for the film synthesized using 20 wt% H₂O in the electrolyte. The extrapolation of the straight line to zero absorption gives the effective band gap energy (E_g) value of approximately 2.25 eV, which is significantly lower than that of TiO₂ anatase (~3.2 eV) (Li et al., 2013). The low band gap value is explained by the presence of vanadium oxide that can extend the absorption band into the visible region. Compared to the color of as-formed Ti–6Al–4V alloy in **Figure 5A**, this result is in agreement with the EDS analysis and the appearance of yellow-green color in the annealed sample at 500°C for 3 h as shown in **Figure 5B**. The color reflected on the annealed TiO₂ NTs sample at 20 wt% H₂O can be determined through the UV absorption spectra. As seen, the lowest absorption spectra is approximately 500 nm, reflecting a yellow-green color. In the agreement with the previous findings, the V-doped TiO₂ materials were prepared by both sol-gel technique and liquid phase deposition (LPD) reported that the presence of V can widen the absorption threshold wavelength to 650 nm (Gu et al., 2007; Zhou et al., 2010). In **Figure 5A** is presented a photo of the sample before annealing.

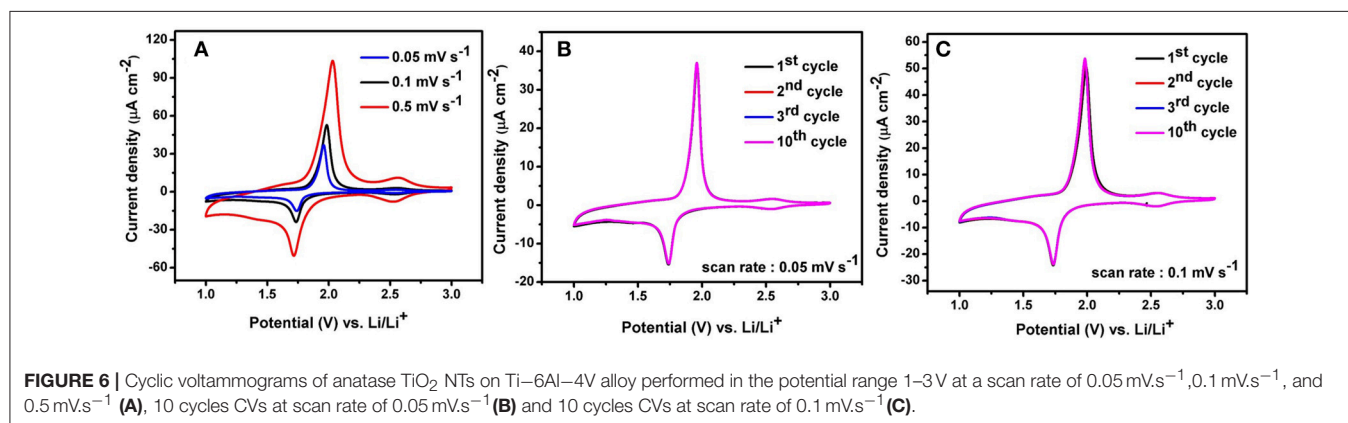
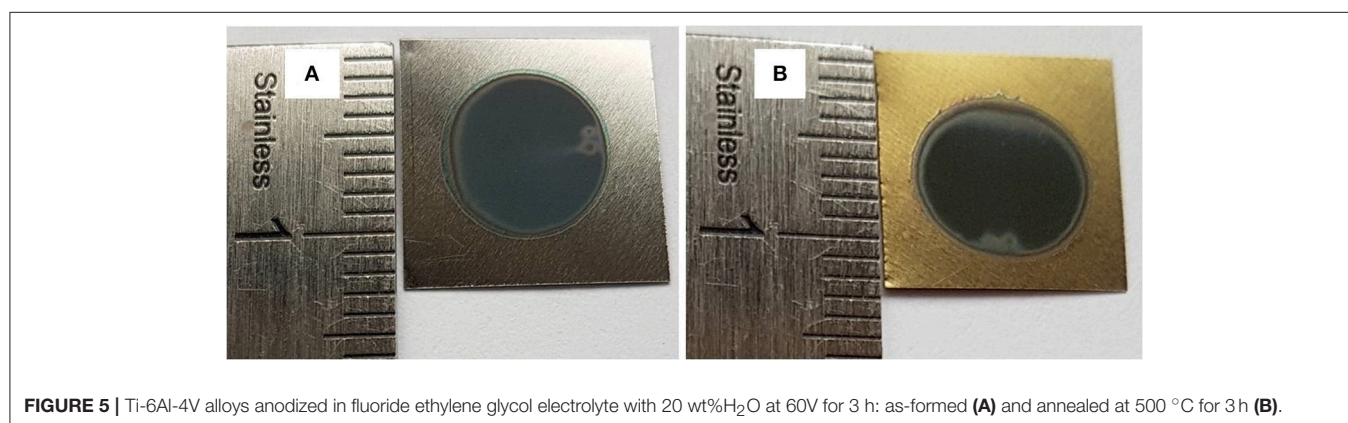
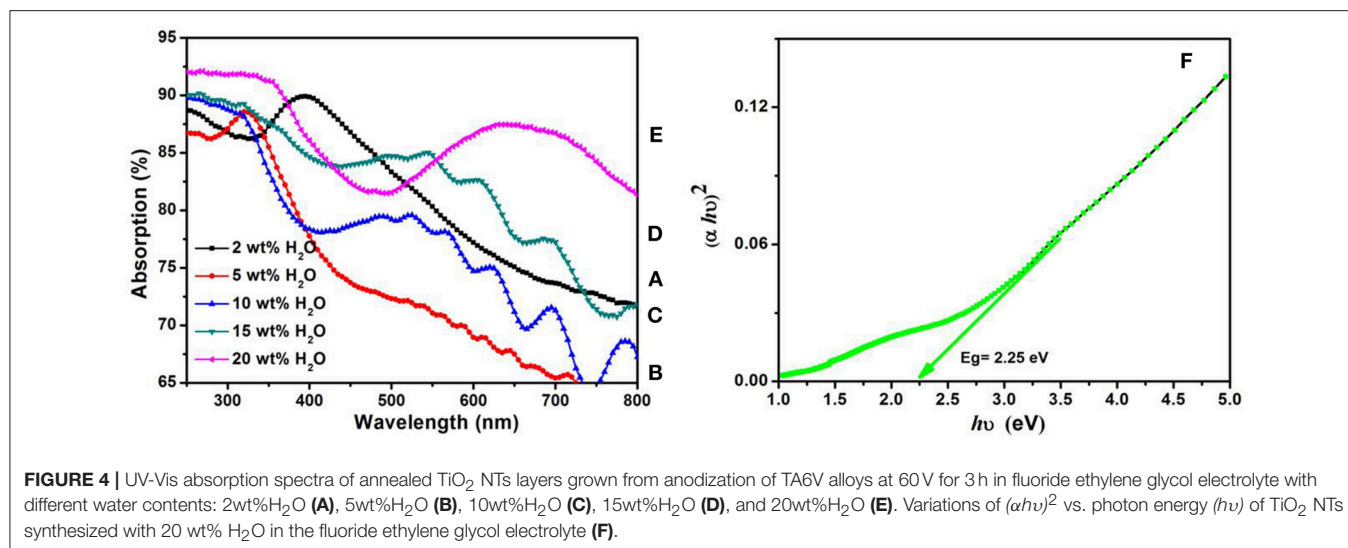
Electrochemical Performance

In this work, self-organized TiO₂ NTs fabricated from TA6V alloy containing α and β phase are investigated as a potential anode materials for Li-ion microbatteries. The electrochemical performance of TiO₂ NTs synthesized using ethylene glycol electrolyte containing 20 wt% H₂O is elucidated through cyclic voltammetry (CV) to analyse the charging and discharging mechanisms during cycling. The anodic and cathodic peaks obtained during the measurements represent the possible phase

transformations or redox reactions with the electrodes (Heinze, 1984). The TiO₂ NTs on TA6V alloy was tested at various scanning rates (0.05, 0.1 and 0.5 mV.s⁻¹) between 1 and 3 V vs. Li/Li⁺ at room temperature, as displayed in **Figure 6A**. Two distinct cathodic and anodic peaks are observed for all scan rates, corresponding to the lithium insertion (Ti⁴⁺ → Ti³⁺) and extraction (Ti³⁺ → Ti⁴⁺) in anatase (Li et al., 2012). At a scan rate of 0.05 mV.s⁻¹, the cathodic peak centered at ~1.74 V vs. Li/Li⁺ and the anodic peak centered at 1.96 V vs. Li/Li⁺ show a peak potential separation (ΔE_p) of 0.22 V. The cathodic and anodic peak slightly shifted to 1.73 V vs. Li/Li⁺ and 1.97 V vs. Li/Li⁺, respectively at 0.1 mV.s⁻¹, showing the ΔE_p of 0.24 V. Further higher scan rate of 0.5 mV.s⁻¹, the cathodic and anodic peaks are significantly shifted to ~1.71 V vs. Li/Li⁺ and ~2.03 V vs. Li/Li⁺, respectively with the ΔE_p of 0.32 V. Obviously, as the scan rate was increased, the displacement current increased due to the fact that the over potential become higher.

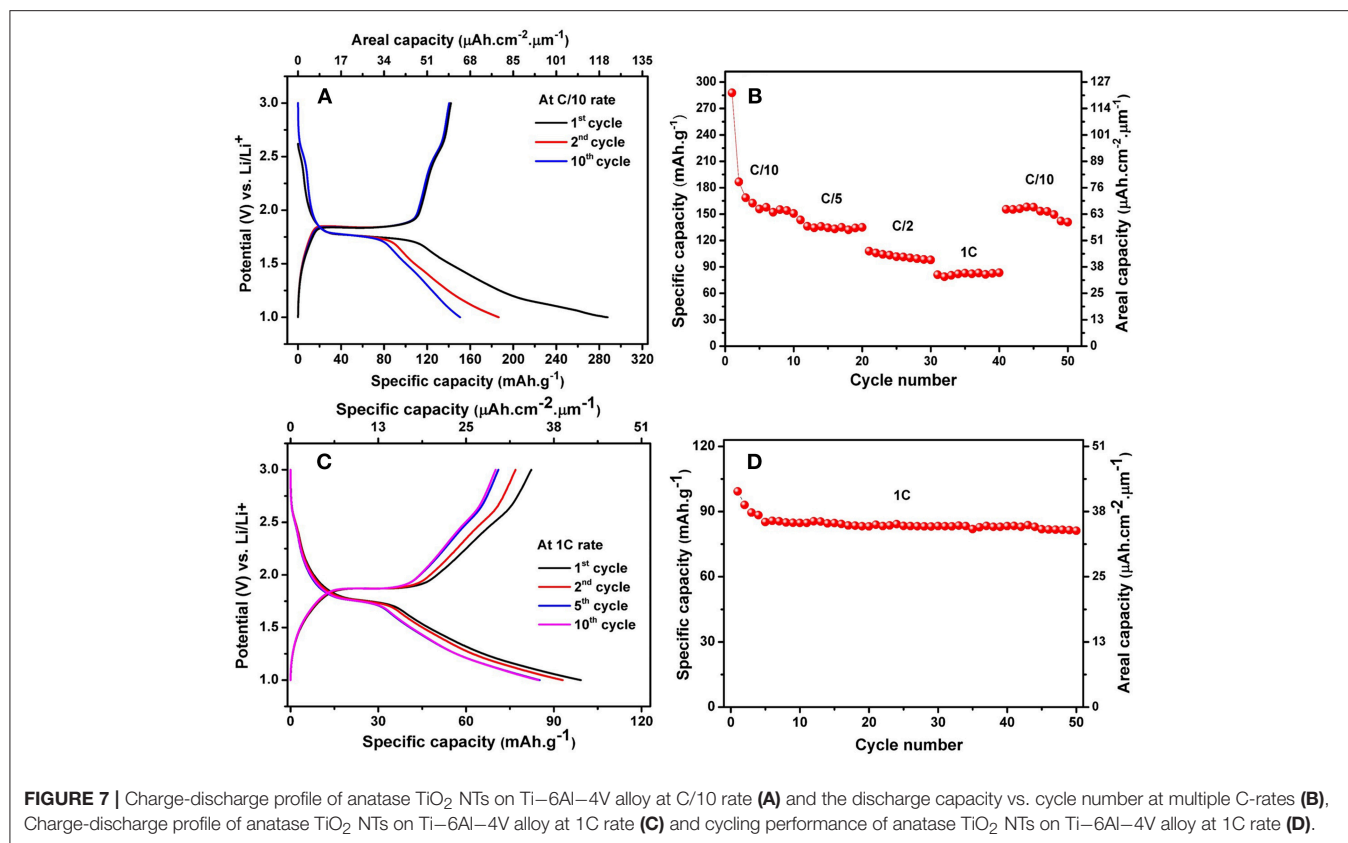
The separation between the cathodic and anodic peaks indicated the extent of polarization. Hence, the slow scan rate is selected to establish an electrochemical equilibrium between the active species due to the fast scan rate might provoke peak identification more difficult (Plylahan et al., 2015). In addition to the main peaks, an additional peak pair at a potential of ~2.55 V vs. Li/Li⁺ with a low current density is showed up in the reduction and oxidation potential at three different scan rates. It is due to the presence of an electrochemically active vanadium oxide with low valence state of vanadium such as VO₂ phase (Mai et al., 2010; Mattelaer et al., 2017). The formation of nanotubes on two phases ($\alpha + \beta$) titanium alloys leads to the selective dissolution of the elements and the different reactions rates at different phases, yielding VO₂ and Al₂O₃ phases. Considering the peak intensity of VO₂ with respect to anatase TiO₂ NTs, it is assumed that the VO₂ phase might not contribute significantly to the storage performance of the electrode. Apart from both peak pairs, no additional peak for the Al₂O₃ phase can be detected in the CVs curves as this phase is probably to be electrochemically inactive. Furthermore, cyclic voltammograms at low scan rate of both 0.05 and 0.1 mV.s⁻¹ for 10 cycles reveal a good stability of the electrode which is attested by no peak shifting (see **Figures 6B,C**). The main cathodic and anodic peaks can be clearly identified up to the 10th cycle.

The charge-discharge behaviors of the alloyed TiO₂ NTs were examined by galvanostatic tests between cut-off voltages of 1 and 3 V vs. Li/Li⁺. The results are shown in **Figure 7A**. It is found that in the first discharge process, there is a short plateau at ~2.55 V which indicates a very small amount of Li ions inserted into VO₂ phase with a low storage capacity. This plateau is in good accordance with the cyclic voltammogram curve. The potential continuously drops and reaches the large constant plateau at ~1.77 V which is attributed to homogeneous Li insertion into the bulk anatase with a lithium insertion capacity of about 85 mAh.g⁻¹ (36 $\mu\text{Ah.cm}^{-2}.\mu\text{m}^{-1}$). The slope after the plateau, started from ~1.77 V to 1 V has the insertion capacity of 183 mAh.g⁻¹ (77 $\mu\text{Ah.cm}^{-2}.\mu\text{m}^{-1}$), which is attributed to the energy capacity accumulated on the surface of anatase. The lithium extraction capacity is solely about 20 mAh.g⁻¹ within

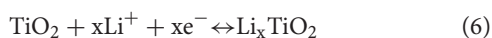


the charging potential window of 1–1.84 V in the first cycle, which is smaller than the capacity in the discharging potential region of 1.77–1 V. This results indicates that the irreversible capacity mainly occurs within the sloped region between 1.77 and 1 V. However, the main voltage plateaus consist of the discharge plateau at ~ 1.77 V vs. Li/Li⁺ and a charge plateau

at ~ 1.84 V vs. Li/Li⁺, resulting in a very small polarization of 0.07 V at C/10 rate. In a good agreement with previous results, the charge plateau at ~ 1.89 V vs. Li/Li⁺ and discharge plateau at ~ 1.75 V vs. Li/Li⁺ with a higher polarization of 0.14 V at C/10 rate are obtained for the self-organized TiO₂ NTs synthesized in a solution of ethylene glycol containing 1.0 wt% H₂O and



2 wt% NH₄F (Prosini et al., 2013). The smaller difference of the charge and discharge plateaus indicates the better electrode reaction kinetics and better rate performance. The reversible Li⁺ insertion into TiO₂ NTs can be written according to Equation (6) (Djenizian et al., 2011).



Taking the middle points between these two plateaus, the average working potentials of cell were determined to be ~ 1.80 V vs. Li/Li⁺. The high working potential of the nanotubes is an advantage to avoid the electrolyte reduction and limit the formation of a solid electrolyte interphase (SEI) layer on the surface of the electrode (Xu et al., 2007).

The electrochemical reaction at the anode is based on the reduction of Ti⁴⁺ to Ti³⁺ and the Li⁺ insertion into the TiO₂ NTs. Lithium ions can be inserted reversibly into anatase TiO₂ to form Li_{0.5}TiO₂, giving a theoretical specific capacity of 168 mAh.g⁻¹ while the theoretical capacity of amorphous TiO₂ NTs is 335 mAh.g⁻¹ for the insertion of one Li per Ti unit (Auer et al., 2018). In this study, the obtained initial discharge and charge capacities of the electrodes are 288 mAh.g⁻¹ (122 $\mu\text{Ah.cm}^{-2}.\mu\text{m}^{-1}$) and 142 mAh.g⁻¹ (60 $\mu\text{Ah.cm}^{-2}.\mu\text{m}^{-1}$), corresponding to the lithium insertion coefficient of 0.86 and 0.42, respectively with a relatively low initial coulombic efficiency of 49.30%. A high capacity of anatase TiO₂ NTs in the first few

initial cycles is probably due to the presence of the remaining amorphous nanotubes (Prosini et al., 2013).

For the subsequent cycles, the discharge capacity values recorded in the 2nd and 10th cycles are 186 and 150 mAh.g⁻¹ with an improved coulombic efficiency of 76.34 and 94.67%, respectively. The capacity fading from the 2nd to the 10th cycle can be attributed to an irreversible reaction of Li⁺ ions with OH groups existing on the surface of nanotubes at low voltages (Ferrari et al., 2017). In addition, the initial capacity loss may also be caused by the interfacial reaction between the residual traces of water on the surface of the nanotubes and lithium salt in the electrolyte combined with the presence of structural defects (Hanzu et al., 2011; Chung et al., 2015). However, the cycling retention continuously improved after first few cycles, thereby coulombic efficiency approaches 100%.

The cells were cycled at multiple C-rates as presented in **Figure 7B**. TiO₂ NTs electrode gives a stable capacity of 150 mAh.g⁻¹ (63 $\mu\text{Ah.cm}^{-2}.\mu\text{m}^{-1}$) at C/10, 134 mAh.g⁻¹ (56 $\mu\text{Ah.cm}^{-2}.\mu\text{m}^{-1}$) at C/5, 101 mAh.g⁻¹ (43 $\mu\text{Ah.cm}^{-2}.\mu\text{m}^{-1}$) at C/2 and 83 mAh.g⁻¹ (35 $\mu\text{Ah.cm}^{-2}.\mu\text{m}^{-1}$) at 1C. The capacity can be recovered after cycling at C/10 rate over 50 cycles. We noted that the capacity loss at C/10 rate after cycling at fast kinetic rates is attributed to the hindered migration of Li⁺ ions within the TiO₂ NTs system due to the presence of other crystalline phases. However, it can be observed that the capacity of two last cycles are enough stable at C/10 rate, hence we assumed the discharge capacities stabilize

after few initial cycles. To prove the cycling stability of the TiO₂ NTs, galvanostatic charge-discharge were performed at 1C rate up to 50 cycles (Figures 7C,D). The results thus clearly show a good cycling stability of the TiO₂ NTs electrodes that can deliver a reversible capacity of 82 mAh.g⁻¹ (34 μAh.cm⁻².μm⁻¹).

CONCLUSION

In summary, self-organized TiO₂ NTs have been successfully synthesized via anodization of Ti–6Al–4V alloy at 60 V for 3 h in fluoride ethylene glycol electrolyte at various water contents (2 wt% up to 20 wt% H₂O). Significant differences in morphological structure of TiO₂ NTs were obtained. At low water content, a honeycomb and porous structure is formed on the surface due to the presence of both α and β phases in the Ti–6Al–4V alloy leading to a dissimilar non-uniform etching. Remarkably, self-organized TiO₂ NTs could be formed uniformly across both α and β phases at 20 wt% H₂O. The optical properties and electrochemical performance of the anodized TiO₂ NTs carrying 20 wt% H₂O have been investigated. The anatase TiO₂ NTs offers a low band gap value equal to 2.25 eV due to the presence

of vanadium oxide in the structure that widens the threshold of absorption wavelength into the visible region. Moreover, galvanostatic charge-discharge tests exhibited a good capacity of 82 mAh.g⁻¹ (34 μAh.cm⁻².μm⁻¹) at 1C rate over 50 cycles. These results show that the self organized TiO₂ NTs grown from TA6V alloy can be considered as competitive anode materials for Li-ion microbatteries, as well as other potential applications in gas sensors, solar cells, and photocatalysis.

AUTHOR CONTRIBUTIONS

HF and VS performed experiments, analyzed the experimental results, and wrote the manuscript. DH, MB, FV, ME, MP, and TD discussed experimental results. All the authors contributed to the reading of paper and gave advice on the revision of the manuscript.

FUNDING

This work is carried out with the contribution of the cooperation project No: 16 MDU 970; Mixed Evaluation and Prospective Commission-Hubert Curien Program (CMEP-PHC) TASSILI.

REFERENCES

- Armstrong, A. R., Armstrong, G., Canales, J., García, R., and Bruce, P. G. (2005). Lithium-ion intercalation into TiO₂-B nanowires. *Adv. Mater.* 17, 862–865. doi: 10.1002/adma.200400795
- Auer, A., Steiner, D., Portenkirchner, E., and Kunze-Liebhäuser, J. (2018). Nonequilibrium phase transitions in amorphous and anatase TiO₂ nanotubes. *ACS Appl. Energy Mater.* 1, 1924–1929. doi: 10.1021/acsaem.7b00319
- Benea, L., Mardare-Danaila, E., Mardare, M., and Celis, J.-P. (2014). Preparation of titanium oxide and hydroxyapatite on Ti–6Al–4V alloy surface and electrochemical behaviour in bio-simulated fluid solution. *Corros. Sci.* 80, 331–338. doi: 10.1016/j.corsci.2013.11.059
- Black, J., and Hastings, G. (2013). *Handbook of Biomaterial Properties*. London: Chapman & Hall; Springer Science and Business Media.
- Chang, Y. C., Peng, C. W., Chen, P. C., Lee, C. Y., and Chiu, H. T. (2015). Bio-ingredient assisted formation of porous TiO₂ for Li-ion battery electrodes. *RSC Adv.* 5, 34949–34955. doi: 10.1039/C5RA04896F
- Chen, Y. W., Chang, J. Y., and Moongraksathum, B. (2015). Preparation of vanadium-doped titanium dioxide neutral sol and its photocatalytic applications under UV light irradiation. *J. Taiwan Inst. Chem. Eng.* 52, 140–146. doi: 10.1016/j.jtice.2015.02.006
- Choi, J., Park, H., and Hoffmann, M. R. (2009). Effects of single metal-ion doping on the visible-light photoreactivity of TiO₂. *J. Phys. Chem. C*, 114, 783–792. doi: 10.1021/jp908088x
- Chung, D. Y., Chung, Y.-H., Kim, S., Lim, J. W., Lee, K. J., Jung, N., et al. (2015). Understanding interface between electrode and electrolyte: organic/inorganic hybrid design for fast ion conductivity. *J. Phys. Chem. C*, 119, 9169–9176. doi: 10.1021/acs.jpcc.5b02075
- Das, S. K., Gnanavel, M., Patel, M. U. M., Shivakumara, C., and Bhattacharyya, A. J. (2011). Anomolously high lithium storage in mesoporous nanoparticulate aggregation of Fe³⁺ doped anatase titania. *J. Electrochem. Soc.* 158:A1290. doi: 10.1149/2.029112jes
- Djenizian, T., Hanzu, I., and Knauth, P. (2011). Nanostructured negative electrodes based on titania for Li-ion microbatteries. *J. Mater. Chem.* 21, 9925–9937. doi: 10.1039/C0JM04205F
- Duan, J., Hou, H., Liu, X., Yan, C., Liu, S., Meng, R., et al. (2016). In situ Ti³⁺-doped TiO₂ nanotubes anode for lithium ion battery. *J. Porous Mater.* 23, 837–843. doi: 10.1007/s10934-016-0139-6
- Ellis, B. L., Knauth, P., and Djenizian, T. (2014). Three-dimensional self-supported metal oxides for advanced energy storage. *Adv. Mater.* 26, 3368–3397. doi: 10.1002/adma.201306126
- Fang, H. T., Liu, M., Wang, D. W., Sun, T., Guan, D. S., Li, F., et al. (2009). Comparison of the rate capability of nanostructured amorphous and anatase TiO₂ for lithium insertion using anodic TiO₂ nanotube arrays. *Nanotechnology* 20:225701. doi: 10.1088/0957-4484/20/22/225701
- Ferrari, I. V., Braglia, M., Djenizian, T., Knauth, P., and Di Vona, M. L. (2017). Electrochemically engineered single Li-ion conducting solid polymer electrolyte on titania nanotubes for microbatteries. *J. Power Sources* 353, 95–103. doi: 10.1016/j.jpowsour.2017.03.141
- Gibrán, K., Ibadurrahman, M., and Slamet. (2018). Effect of electrolyte type on the morphology and crystallinity of TiO₂ nanotubes from Ti–6Al–4V anodization. *IOP Conf. Ser. Earth Environ. Sci.* 105:012038. doi: 10.1088/1755-1315/105/1/012038
- Gu, D.-E., Yang, B.-C., and Hu, Y.-D. (2007). A novel method for preparing V-doped titanium dioxide thin film photocatalysts with high photocatalytic activity under visible light irradiation. *Catal. Lett.* 118, 254–259. doi: 10.1007/s10562-007-9179-5
- Hanzu, I., Djenizian, T., and Knauth, P. (2011). Electrical and point defect properties of TiO₂ nanotubes fabricated by electrochemical anodization. *J. Phys. Chem. C*, 115, 5989–5996. doi: 10.1021/jp1111982
- Heinze, J. (1984). Cyclic voltammetry—“Electrochemical Spectroscopy”. new analytical methods(25). *Angew. Chem. Int. Ed. Engl.* 23, 831–847. doi: 10.1002/anie.198408313
- Hoffmann, M. R., Martin, S. T., Choi, W., and Bahnemann, D. W. (1995). Environmental applications of semiconductor photocatalysis. *Chem. Rev.* 95, 69–96. doi: 10.1021/cr00033a004
- Jo, C.-I., Jeong, Y.-H., Choe, H.-C., and Brantley, W. A. (2013). Hydroxyapatite precipitation on nanotubular films formed on Ti–6Al–4V alloy for biomedical applications. *Thin Solid Films.* 549, 135–140. doi: 10.1016/j.tsf.2013.09.095
- Kyeremateng, N. A., Plylahan, N., dos Santos, A. C., Taveira, L. V., Dick, L. F., and Djenizian, T. (2013a). Sulfidated TiO₂ nanotubes: a potential 3D cathode material for Li-ion micro batteries. *Chem. Commun.* 49, 4205–4207. doi: 10.1039/c2cc36857a
- Kyeremateng, N. A., Vacandio, F., Sougrati, M. T., Martinez, H., Jumas, J. C., Knauth, P., et al. (2013b). Effect of Sn-doping on the electrochemical behaviour

- of TiO₂ nanotubes as potential negative electrode materials for 3D Li-ion micro batteries. *J. Power Sources*. 224, 269–277. doi: 10.1016/j.jpowsour.2012.09.104
- Li, H., Martha, S. K., Unocic, R. R., Luo, H., Dai, S., and Qu, J. (2012). High cyclability of ionic liquid-produced TiO₂ nanotube arrays as an anode material for lithium-ion batteries. *J. Power Sources* 218, 88–92. doi: 10.1016/j.jpowsour.2012.06.096
- Li, J., Du, Z., Ruther, R. E., An, S. J., David, L. A., Hays, K., et al. (2017). Toward low-cost, high-energy density, and high-power density lithium-ion batteries. *JOM-US69*, 1484–1496. doi: 10.1007/s11837-017-2404-9
- Li, L., Liu, C. Y., and Liu, Y. (2009). Study on activities of vanadium (IV/V) doped TiO₂ (R) nanorods induced by UV and visible light. *Mater. Chem. Phys.* 113, 551–557. doi: 10.1016/j.matchemphys.2008.08.009
- Li, Z., Ding, D., Liu, Q., and Ning, C. (2013). Hydrogen sensing with Ni-doped TiO₂ Nanotubes. *Sensors* 13, 8393–8402. doi: 10.3390/s130708393
- Lin, S.-H., Ou, C.-C., Su, M.-D., and Yang, C.-S. (2013). Photo-catalytic behavior of vanadia incorporated titania nanoparticles. *Catal. Sci. Technol.* 3, 2081–2091. doi: 10.1039/c3cy00053b
- Long, M., and Rack, H. J. (1998). Titanium alloys in total joint replacement—a materials science perspective. *Biomaterials* 19, 1621–1639. doi: 10.1016/s0142-9612(97)00146-4
- Luo, B., Yang, H., Liu, S., Fu, W., Sun, P., Yuan, M., et al. (2008). Fabrication and characterization of self-organized mixed oxide nanotube arrays by electrochemical anodization of Ti–6Al–4V alloy. *Mater. Lett.* 62, 4512–4515. doi: 10.1016/j.matlet.2008.08.015
- Macak, J. M., Tsuchiya, H., Taveira, L., Ghicov, A., and Schmuki, P. (2005). Self-organized nanotubular oxide layers on Ti-6Al-7Nb and Ti-6Al-4V formed by anodization in NH₄F solutions. *J. Biomed. Mater. Res. Part A* 75, 928–933. doi: 10.1002/jbm.a.30501
- Mai, L., Xu, L., Han, C., Xu, X., Luo, Y., Zhao, S., et al. (2010). Electrospun ultralong hierarchical vanadium oxide nanowires with high performance for lithium ion batteries. *Nano Lett.* 10, 4750–4755. doi: 10.1021/nl103343w
- Mane, R. S., Lee, W. J., Pathan, H. M., and Han, S. H. (2005). Nanocrystalline TiO₂/ZnO thin films: fabrication and application to dye-sensitized solar cells. *J. Phys. Chem. B* 109, 24254–24259. doi: 10.1021/jp0531560
- Mattelaer, F., Geryl, K., Rampelberg, G., Dendooven, J., and Detavernier, C. (2017). Amorphous and crystalline vanadium oxides as high-energy and high-power cathodes for three-dimensional thin-film lithium ion batteries. *ACS Appl. Mater. Interfaces* 9, 13121–13131. doi: 10.1021/acsami.6b16473
- Matytkina, E., Hernandez-López, J. M., Conde, A., Domingo, C., de Damborenea, J. J., and Arenas, M. A. (2011). Morphologies of nanostructured TiO₂ doped with F on Ti–6Al–4V alloy. *Electrochim. Acta* 56, 2221–2229. doi: 10.1016/j.electacta.2010.11.069
- Moravec, H., Vandrovčová, M., Chotová, K., Fojt, J., Pruchová, E., Joska, L., et al. (2016). Cell interaction with modified nanotubes formed on titanium alloy Ti-6Al-4V. *Mater. Sci. Eng. C*. 65, 313–322. doi: 10.1016/j.msec.2016.04.037
- Morozová, M., Kluson, P., Krysa, J., Vesely, M., Dzik, P., and Solcova, O. (2012). Electrochemical properties of TiO₂ electrode prepared by various methods. *Procedia. Eng.* 42, 573–580. doi: 10.1016/j.proeng.2012.07.450
- Nešić, J., Manojlović, D. D., Anđelković, I., Dojčinović, B. P., Vulić, P. J., Krstić, J., and et Roglić, G. M. (2013). Preparation, characterization and photocatalytic activity of lanthanum and vanadium co-doped mesoporous TiO₂ for azo-dye degradation. *J. Mol. Catal. A: Chem.* 378, 67–75. doi: 10.1016/j.molcata.2013.05.018
- Ortiz, G. F., Hanzu, I., Djenizian, T., Lavela, P., Tirado, J. L., and Knauth, P. (2008). Alternative Li-ion battery electrode based on self-organized titania nanotubes. *Chem. Mater.* 21, 63–67. doi: 10.1021/cm801670u
- Ortiz, G. F., Hanzu, I., Knauth, P., Lavela, P., Tirado, J. L., and Djenizian, T. (2009). TiO₂ nanotubes manufactured by anodization of Ti thin films for on-chip Li-ion 2D microbatteries. *Electrochim. Acta* 54, 4262–4268. doi: 10.1016/j.electacta.2009.02.085
- Panda, S. K., Yoon, Y., Jung, H. S., Yoon, W. S., and Shin, H. (2012). Nanoscale size effect of titania (anatase) nanotubes with uniform wall thickness as high performance anode for lithium-ion secondary battery. *J. Power Sources*. 204:162167. doi: 10.1016/j.jpowsour.2011.12.048
- Pansila, P., Witit-Anun, N., and Chaiyakun, S. (2012). Influence of sputtering power on structure and photocatalyst properties of DC magnetron sputtered TiO₂ thin film. *Procedia. Eng.* 32, 862–867. doi: 10.1016/j.proeng.2012.02.024
- Pikul, J. H., Zhang, H. G., Cho, J., Braun, P. V., and King, W. P. (2013). High-power lithium ion microbatteries from interdigitated three-dimensional bicontinuous nanoporous electrodes. *Nat. Commun.* 4:1732. doi: 10.1038/ncomms2747
- Pylahan, N., Demoulin, A., Chrystelle Lebouin, C. L., Knauth, P., and Djenizian, T. (2015). Mechanism study of Li⁺ insertion into titania nanotubes. *RSC Adv.* 5, 28474–28477. doi: 10.1039/c5ra03759j
- Pylahan, N., Kyeremateng, N. A., Eyraud, M., Dumur, F., Martinez, H., Santinacci, L., et al. (2012). Highly conformal electrodeposition of copolymer electrolytes into titania nanotubes for 3D Li-ion batteries. *Nanoscale Res. Lett.* 7:349. doi: 10.1186/1556-276x-7-349
- Pylahan, N., Letiche, M., Barr, M. K. S., and Djenizian, T. (2014). All-solid-state lithium-ion batteries based on self-supported titania nanotubes. *Electrochim. Commun.* 43, 121–124. doi: 10.1016/j.electcom.2014.03.029
- Prosini, P. P., Cento, C., and Pozio, A. (2013). Lithium-ion batteries based on titanium oxide nanotubes and LiFePO₄. *J. Solid State Electrochem.* 18, 795–804. doi: 10.1007/s10008-013-2324-8
- Reszczynska, J., Grzyb, T., Sobczak, J. W., Lisowski, W., Gazda, M., Ohtani, B., et al. (2014). Lanthanide co-doped TiO₂: the effect of metal type and amount on surface properties and photocatalytic activity. *Appl. Surf. Sci.* 307, 333–345. doi: 10.1016/j.apsusc.2014.03.199
- Salian, G. D., Koo, B. M., Lefevre, C., Cottineau, T., Lebouin, C., Tesfaye, A. T., et al. (2018). Niobium alloying of self-organized TiO₂ nanotubes as an anode for lithium-ion microbatteries. *Adv. Mater. Technol.* 3 :1700274. doi: 10.1002/admt.201700274
- Salian, G. D., Lebouin, C., Demoulin, A., Lepihin, M. S., Maria, S., Galeyeva, A. K., et al. (2017). Electrodeposition of polymer electrolyte in nanostructured electrodes for enhanced electrochemical performance of thin-film Li-ion microbatteries. *J. Power Sources*, 340, 242–246. doi: 10.1016/j.jpowsour.2016.11.078
- Sopha, H., Salian, G. D., Zazpe, R., Prikryl, J., Hromadko, L., Djenizian, T., et al. (2017). ALD Al₂O₃-coated TiO₂ nanotube layers as anodes for lithium-ion batteries. *ACS Omega* 2, 2749–2756. doi: 10.1021/acsomega.7b00463
- Sugiawati, V. A., Vacandio, F., Eyraud, M., Knauth, P., and Djenizian, T. (2016). Porous NASICON-Type Li₃Fe₂(PO₄)₃ thin film deposited by rf sputtering as cathode material for li-ion microbatteries. *Nanoscale Res. Lett.* 11:365. doi: 10.1186/s11671-016-1574-7
- Sugiawati, V. A., Vacandio, F., Knauth, P., and Djenizian, T. (2018). Sputter-deposited amorphous LiCuPO₄ thin film as cathode material for li-ion microbatteries. *Chem. Select* 3, 405–409. doi: 10.1002/slct.201702429
- Tang, D., Wang, Y., Zhao, Y., Yang, Y., Zhang, L., and Mao, X. (2014). Effect of the composition of Ti alloy on the photocatalytic activities of Ti-based oxide nanotube arrays prepared by anodic oxidation. *Appl. Surf. Sci.* 319, 181–188. doi: 10.1016/j.apsusc.2014.07.149
- Xiong, W., Xia, Q., and Xia, H. (2014). Three-dimensional self-supported metal oxides as cathodes for microbatteries. *Funct. Mater. Lett.* 7:1430003. doi: 10.1142/S1793604714300035
- Xu, J., Jia, C., Cao, B., and Zhang, W. F. (2007). Electrochemical properties of anatase TiO₂ nanotubes as an anode material for lithium-ion batteries. *Electrochim. Acta*, 52, 8044–8047. doi: 10.1016/j.electacta.2007.06.077
- Yu, C., Bai, Y., Yan, D., Li, X., and Zhang, W. (2014). Improved electrochemical properties of Sn-doped TiO₂ nanotube as an anode material for lithium ion battery. *J. Solid State Chem.* 18, 1933–1940. doi: 10.1007/s10008-014-2436-9
- Zhou, W., Liu, Q., Zhu, Z., and Zhang, J. (2010). Preparation and properties of vanadium-doped TiO₂ photocatalysts. *J. Phys. D: Appl. Phys.* 43, 035301. doi: 10.1088/0022-3727/43/3/035301

Conflict of Interest Statement: The authors declare that the research was conducted in the absence of any commercial or financial relationships that could be construed as a potential conflict of interest.

Copyright © 2019 Fraucene, Sugiawati, Hatem, Belkaid, Vacandio, Eyraud, Pasquinielli and Djenizian. This is an open-access article distributed under the terms of the Creative Commons Attribution License (CC BY). The use, distribution or reproduction in other forums is permitted, provided the original author(s) and the copyright owner(s) are credited and that the original publication in this journal is cited, in accordance with accepted academic practice. No use, distribution or reproduction is permitted which does not comply with these terms.